iPSC-derived lung and lung cancer organoid model to evaluate cisplatin encapsulated autologous iPSC-derived mesenchymal stromal cell-isolated extracellular vesicles

Caroline Küstermann[1]*, Karīna Narbute[1], Valērija Movčana[1], Vadims Parfejevs[2], Fēlikss Rūmnieks[1], Pauls Kauķis[1], Miks Priedols[1], Rihards Mikilps-Mikgelbs[3], Marija Mihailova[4], Santa Andersone[4], Aigars Dzalbs[4], Cristina Bajo-Santos[1], Alvils Krams[3] and Arturs Abols[1]

Abstract

Background Lung cancer remains a leading cause of cancer-related mortality globally. Although recent therapeutic advancements have provided targeted treatment approaches, the development of resistance and systemic toxicity remain primary concerns. Extracellular vesicles (EVs), especially those derived from mesenchymal stromal cells (MSC), have gained attention as promising drug delivery systems, offering biocompatibility and minimal immune responses. Recognizing the limitations of conventional 2D cell culture systems in mimicking the tumor microenvironment, this study aims to describe a proof-of-principle approach for using patient-specific organoid models for both lung cancer and normal lung tissue and the feasibility of employing autologous EVs derived from induced pluripotent stem cell (iPSC)-MSC in personalized medicine approaches.

Methods First, we reprogrammed healthy fibroblasts into iPSC. Next, we differentiated patient-derived iPSC into branching lung organoids (BLO) and generated patient-matched lung cancer organoids (LCO) from patient-derived tumor tissue. We show a streamlined process of MSC differentiation from iPSC and EV isolation from iPSC-MSC, encapsulated with 0.07 µg/mL of cytotoxic agent cisplatin and applied to both organoid models. Cytotoxicity of cisplatin and cisplatin-loaded EVs was recorded with LDH and CCK8 tests.

Results Fibroblast-derived iPSC showed a normal karyotype, pluripotency staining, and trilineage differentiation. iPSC-derived BLO showed expression of lung markers, like TMPRSS2 and MUC5A while patient-matched LCO showed expression of Napsin and CK5. Next, we compared the effects of iPSC-MSC derived EVs loaded with cisplatin against empty EVs and cisplatin alone in lung cancer organoid and healthy lung organoid models. As expected, we found a cytotoxic effect when LCO were treated with 20 µg/mL cisplatin. Treatment of LCO and BLO with empty EVs resulted in a cytotoxic effect after 24 h. However, EVs loaded with 0.07 µg/mL cisplatin failed to induce any cytotoxic effect in both organoid models.

*Correspondence:
Caroline Küstermann
caroline.kustermann@biomed.lu.lv
Full list of author information is available at the end of the article

Conclusion We report on a proof-of-principle pipeline towards using autologous or allogeneic iPSC-MSC EVs as drug delivery tests for lung cancer in future. However, due to the time and labor-intensive processes, we conclude that this pipeline might not be feasible for personalized approaches at the moment.

Keywords iPSC, Cisplatin, EVs, Lung cancer, Organoids

Introduction

The World Health Organization (WHO) predicts that, within the next forty years, cancer will surpass ischemic heart disease (IHD) as the primary cause of death, demonstrating a projected increase of more than two-fold from 2016 to 2060 [1]. With 2.2 million new cases and 1.8 million deaths worldwide in 2020, lung cancer is one of the most common types of cancer and a leading cause of cancer-related deaths worldwide [2]. Non-small cell lung cancer (NSCLC) accounts for approximately 85% of all lung cancer cases [3].

In the context of lung cancer treatment, while recent breakthroughs in targeted molecular therapy and immuno-oncology have transformed the field, cytotoxic chemotherapy remains the primary therapeutic option [4]. Traditional systemic administration of chemotherapy drugs, such as cisplatin, often leads to significant toxicity due to the lack of specificity of cancer cells [5]. In recent years, targeted approaches have emerged, particularly in cases with driver mutations such as *EGFR* exon 19 deletion or *ALK* gene translocation [6]. However, it is important to note that almost all targeted therapy approaches eventually develop resistance, rendering the therapy ineffective [7]. Furthermore, targeted therapy is only suitable for a small percentage of patients, as not all cases exhibit predominant driver mutations [8]. Hence, an urgent requirement exists for drug delivery systems with the capacity to transport drugs directly to tumors, thus mitigating systemic toxicity. Innovative strategies, such as nanoparticle-based delivery systems, hold great promise for addressing this need.

Extracellular vesicles (EVs) are bilipid membrane vesicles ranging in size of 30 nm-10 μm that cells release into the extracellular space. They play a pivotal role in intercellular communication by transporting specific cargoes, including lipids, proteins, and nucleic acids, and participating in immune responses during both normal physiological and pathological conditions [9, 10]. EVs have attained substantial attention as potential drug delivery systems capable of conveying proteins, miRNAs, and various therapeutic agents, such as cytotoxic drugs; thereby modulating cellular responses to control or delay disease progression [11]. In addition, several in vivo studies have demonstrated that EVs are well-tolerated and biocompatible, evoking minimal immune reactions [12].

Over the past decade, extensive research has focused on MSC, owing to their ability to migrate and engraft in target tissues [13]. Recent research, however, has shown that only a small number of MSC reach their target tissues after being given intravenously [14, 15]. This suggests that paracrine actions are the primary cause of their therapeutic effects. EVs derived from MSC have exhibited therapeutic properties encompassing anti-inflammatory, wound healing, and anti-cancer effects [15–17]. Nonetheless, numerous uncertainties persist regarding the safe and effective translation of EVs from preclinical settings to clinical trials. These challenges include concerns related to comprehensive EV content, safety profiles, and administration-associated toxicity [14].

Lung cancer research has conventionally been carried out in 2D cell culture systems, but these inadequately replicate the complexity of the tumor microenvironment [18]. The advent of organoids has ushered in a new era in lung cancer research, faithfully recapitulating the heterogeneity and pathogenicity of the original tumor [19, 20]. These organoids faithfully replicate the patient's tumor and preserve its genetic and epigenetic landscape, enabling high-throughput drug screenings and the formulation of personalized treatment strategies [21]. Furthermore, patient-derived induced pluripotent stem cell (iPSC) organoids represent a transformative approach to personalized medicine, providing invaluable insights into the drug toxicity and off-target to healthy tissues [22].

Capitalizing on our understanding of the overexpression of various surface proteins in NSCLC, including the chemokine receptor CXCR4 and its ligand stromal cell-derived factor-12 (CXCL12/CXCR4) and EGFR, we can engineer EVs to target these specific proteins and deliver cytotoxic cargo to cancer cells [23]. This innovative approach has the potential to significantly reduce the required effective dosage of therapeutic agents and thereby minimize systemic toxicity [24]. Notably, unlike other nanoparticle delivery systems, autologous EVs derived from a patient's own cells elicit minimal immune responses and exhibit a relatively prolonged half-life in the bloodstream [25]. While drug-loaded EVs have been extensively investigated in various in vitro models, these models often fail to replicate the physiologically relevant tissue architecture and cell-extracellular matrix interactions [26]. Consequently, there is an increasing demand for advanced in vitro systems that can offer a more

Küstermann *et al. Stem Cell Research & Therapy*   (2024) 15:246

Page 3 of 15

precise assessment of the impact of drug-loaded EVs on lung tissue.

Hence, the aim of this investigation was to develop a patient-specific organoid model for lung cancer and normal lung tissue to compare the cytotoxic effects of autologous iPSC-MSC-derived EVs encapsulated with cisplatin to those of empty EVs and cisplatin on its own. This study serves as a feasibility test of a proof of principle to implement fully personalized lung and lung cancer models for autologous MSC drug carrying EV tests.

Methods

Operation material and tumor organoid generation

Patient inclusion criteria were ≥ 18 years, have not had a recent blood transfusion, did not exhibit any other malignancies, treatment-naive NSCLC primary tumor patients, capable of providing written and informed consent. Only patients with large tumors (> 5 cm in diameter) were asked to participate in this study to provide sufficient tumor material without compromising quality of the specimen for pathological examination. Tissue samples were obtained during the scheduled surgical operation with radical intent (Pulmonary lobectomy, bilobectomy or pneumonectomy). Fragment of tumor tissue was excised directly after delivery of surgical specimen, as well as a segment of healthy lung tissue measuring 0.5–2 cm^3, located distally from the tumor site. A portion of this surgical specimen was preserved in cold 10% formalin and dispatched to the pathology laboratory to confirm the presence of NSCLC. The remaining tissue was immediately submerged in Hank's balanced salt solution (HBSS) containing an antibiotic/antimycotic reagent (15,240,096, ThermoFisher) and processed within 12 h post-surgery. In total two patient samples were used for this study. Lung adenocarcinoma organoids from clinical samples were established following the protocol outlined by Li et al., as detailed in STAR Protocols [27]. Briefly, the tumor samples were subjected to a mincing and 1-h digestion process using collagenase type II and DNase I at 37 °C, with continuous agitation at 120 rpm. Subsequently, a 10-min trypsinization step was performed. After digestion, the cell suspension was sieved through a 70-µm strainer to remove larger tissue fragments. The filtered cells were gently mixed with Matrigel, and droplets of 30–50 µL were placed on a preheated 6-well plate. These droplets were inverted for 1 min and then reverted for 10 min in an incubator to solidify. Each well was filled with 2.5 mL of warm organoid culture medium, and any vacant wells were supplemented with sterile PBS to prevent medium evaporation. Organoid cultivation continued until they reached a diameter of 100–150 µm (approximately 2 weeks), after which they were subjected to further analysis.

Cell culture and medium

Healthy patient-derived fibroblasts were isolated from healthy lung tissue as described in the previous section. Patient-derived human lung fibroblasts and irradiated CD1 mouse embryonic fibroblasts (MEFs, A34181, ThermoFisher) were maintained in MEF medium. This medium consisted of high glucose DMEM (#41,966–029, Gibco) supplemented with 10% FCS, 100 U/mL P/S and 2 mM L-Glu. Reprogramming of MEFs was performed in iPSC medium, which was composed of KO-DMEM (Gibco) supplemented with 20% Knockout serum replacement, 100 U/mL P/S, 2 mM L-Glu, 0.1 mM MEM minimal non-essential amino acids (NEAA), 0.1 mM β-Mercaptoethanol, 10 ng/mL bFGF (#100-18B, Preprotech). Feeder-free iPSC culture was conducted on geltrex (A1413201, ThermoFisher) coated plates and in mTeSR$^+$ medium (#85,850, Stemcell Technologies).

Generation and characterization of iPSC and iPSC-MSC

Generation and characterization of iPSC was done following previously published protocol [28] and can be found in Supplementary file 1: methods section 1 (1—6). Generation of iPSC-MSC was performed following protocol by [29] and characterized via fluorescence-activated flow cytometry (FACS). Full method description can be found in Supplementary file 1: methods section 1 (7–8).

Cisplatin-loading into extracellular vesicles

EVs derived from iPSC-MSC were isolated using size exclusion chromatography (SEC) and characterized by transmission electron microscopy (TEM), dsELISA and nanoparticle tracking analysis (NTA). Encapsulation of cisplatin in EVs was assessed using high-performance liquid chromatography (HPLC). EV isolation and characterization was done as described in Supplementary file 1: methods section 2.

Subconfluent iPSC-MSC adherent culture (3×10^5) was exposed to the highest non-toxic concentration of cisplatin (20 µg/mL according to previously obtained data in CCK8 and LDH test; Fig. 3E). After 48 h of incubation, cell media was collected for vesicle extraction. Cell media was centrifuged at $300 \times g$ for 5 min at 4 °C, then supernatant was centrifuged again at $3000 \times g$ for 30 min at 4 °C to eliminate residual cells and debris. Next, supernatant was concentrated to 5 mL using 100 kDa 15 mL centrifugation columns (UFC910024, Merck) at $3000 \times g$ at 4 °C and EVs were isolated, as described in section "EV isolation and characterization", found in Supplementary file 1: methods section 2. Cisplatin cytotoxicity assays (CCK8 and LDH) were performed following manufacturer's

instructions. Details can be found in Supplementary file 1: methods section 3.

Cisplatin quantification

Cisplatin content in vesicles was determined using high-performance liquid chromatography based on a protocol described previously [30]. Briefly, cisplatin encapsulated vesicles were disassembled, centrifuged at 10.000 rpm for 10 min and supernatant was vacuum dried. Pellet was suspended in 100 µL of 0.9% sodium chloride and 10 µL of 50 µg/mL nickel chloride as an internal standard. 100 µL of 1% DDTC in 0.1 M sodium hydroxide solution was added, and samples were incubated at 37 °C for 30 min and extracted with 100 µL chloroform. The mixture was centrifuged at 10.000 rpm for 10 min and the chloroform layer separated. 5 µL of the chloroform layer was injected into the chromatographic system.

Chromatographic conditions

The assay calibration was done using known amounts of cisplatin (from 0.01 to 20 µg/mL). Calibration curves were set up by plotting cisplatin peak area and linear function retrieved to calculate cisplatin content in vesicles. The chromatographic system Shimadzu Prominence with DAD was used. Separation was conducted at 23 °C on a 150 mm × 4.6 mm Altima HP C18 Amide column of 3 µm particle size. The mobile phase was a mixture of water, methanol and acetonitrile (36: 32: 32), with a constant flow of 0.5 mL/min. Detection was performed at 340 nm.

iPSC- derived LCO and BLO exposure to cisplatin and cisplatin loaded EV

BLO and LCO were treated with iPSC-MSC derived EV, EV loaded with cisplatin and cisplatin alone (0.07 µg/ml and 20 µg/ml) for 48 h. To evaluate the effect of autologous EVs encapsulated cisplatin, iPSC-derived BLO and patient-matched LCO were seeded in Matrigel domes and exposed to either 3×10^{10} iPSC-MSC EVs, 3×10^{10} EVs + cispt in total amount or cisplatin alone (20 µg/mL and 0.07 µg/mL). 0.07 µg/mL cisplatin was used as this reflects the cisplatin concentration in encapsulated EVs. RNA was isolated after 48 h of exposure. CCK8 and LDH assays were performed during EV exposure. Details can be found in supplementary file 1: methods section 3.

Image processing and statistical analysis

Confocal microscopy was performed using Leica TCS SP8 laser scanning confocal microscope (Leica Microsystems, Germany). Four laser lines were used: Diode (405 nm) for DAPI and Hoechst, Argon (488 nm) for AlexaFluor488, and HeNe (633 nm) for AlexaFluor647. Z-stacks were scanned using 40x/N.A. 1.25 objective.

Images and Z-stack maximum projections were then processed using Leica Application Suite X software (Leica Microsystems, Germany). Color brightness, color balance and contrast was adjusted for all images using ImageJ software. Figures were assembled using Inkscape 1.2.2. Statistical analyses for all graphs were done in GraphPad Prism 10.1 and comparisons among groups were analyzed using Mann–Whitney test. *p* values < 0.05 were considered significant.

Results

iPSC generation from NSCLC patient-derived lung fibroblasts

To generate healthy iPSC from NSCLC patients, healthy lung tissue was acquired via biopsy from operation samples, dissociated, and cultured in vitro. The attached cells were cultured for 2–3 passages, followed by normal fibroblast confirmation. The cells underwent flow cytometry analysis for CD90 surface marker expression, revealing that 98% of cells expressed CD90. Notably, cells showed an intermediate and high CD90 expression separating them into 2 distinct cell populations (Fig. 1A). Following flow cytometry, healthy lung fibroblasts were transduced with Sendai virus particles carrying *OCT4*, *KLF4*, *SOX2* and *C-MYC*. After 2–3 weeks of co-culture with CD1 MEFs, iPSC colonies emerged and were successfully picked onto geltrex-coated plates (Fig. 1A). Four clones per patient were selected and analyzed for karyotype, pluripotency markers, and trilineage differentiation. The established patient-derived iPSC from LC0008 (Fig. 1B) and LC0001 (Fig. 1C) expressed pluripotency factors such as OCT4, Nanog, SSEA4 and TRA1-60. Clones Fib3iPSC cl20 (LC0008) (Fig. 1D) and Fib2iPSC cl16 (LC0001) (Supplementary file 1: Fig. 1E) exhibited a normal karyotype and were utilized in subsequent differentiations. Differentiation of both clones into mesoderm, endoderm, and ectoderm, showed successful downregulation of *OCT4* on day 5 (mesoderm and endoderm) or day 7 (ectoderm) of differentiation (Fig. 1F, G). The mesoderm-specific gene Brachyury showed a robust upregulation on day 5, while Eomes exhibited a less pronounced upregulation. Endoderm-specific genes *FOXA2* and *SOX17* were prominently upregulated after 5 days of endoderm differentiation in both clones. Ectoderm-specific genes *PAX6* and *NESTIN* showed a notable upregulation after 7 days of ectoderm differentiation compared to iPSC (day 0).

Furthermore, iPSC from LC0001 and LC0008 were examined for the absence of Sendai virus genome and the transgenes (Fig. 1H, I). While transduced fibroblast from day 7 of infection showed the presence of the Sendai virus genome (*SeV*) and the transgenes (*KOS*, *KLF4* and *c-MYC*), the combination of transgenes *KOS* and

KLF4 could not be detected in all iPSC clones. However, the *c-MYC* transgene and *SeV* genome were detected via PCR in 3 out of 6 tested iPSC clones (Fig. 1H, I), with the *C-MYC* transgene persisting longer in the cells. In summary, the selected iPSC clones from LC0001 and LC0008 showed all the hallmarks of successfully reprogrammed cells, establishing fully functional iPSC clones. Consequently, patient-derived iPSC clones (LC0001 cl16 and LC0008 cl20) are considered suitable for differentiation into lung organoids and iPSC-MSC.

iPSC were differentiated into lung organoids and patient-derived lung *cancer* organoids were isolated

To generate healthy patient lung organoids, iPSC clones from LC0001 and LC0008 were subjected to differentiation using a commercial kit (see Methods Sect. 1.6) (Fig. 2A, B). Initially, definitive endoderm differentiation was induced, resulting in the observation of a monolayer of cells on day 1 (Fig. 2A, B, d1 and d2). By day 4 of differentiation, anterior foregut endoderm (AFE) buds emerged on top of the monolayer (Fig. 2A, B, d4). These AFE buds were harvested on day 7 and subsequently cultured in suspension. In suspension culture, AFE buds developed into spheroids (Fig. 2A, B, d15—d22). The spheroids were then seeded into a Matrigel sandwich and cultured until at least day 42 of differentiation. Over this period, densely packed lung organoids (Fig. 2A, B, d23) matured, forming buds with a thin layer of polarized cells by day 49 (Fig. 2A, B, d46 and d49). To validate the differentiation into lung cells, mature iPSC-derived lung organoids were extracted from the Matrigel sandwich, minced, and subjected to immunofluorescence analysis. Mature iPSC-derived lung organoids robustly expressed acetylated α-tubulin, TMPRSS2, MUC5AC and EpCAM (Fig. 2C). Notably, a small percentage of SOX2-expressing cells was observed in lung organoids on day 52 of differentiation. The polarized structure of the lung was compromised due to the mincing process for immunofluorescence staining. Patient-matched lung cancer organoids (LCO) were established using a lung cancer operation sample (Supplementary file 1: Fig. 1) and following the protocol by [27] (Fig. 2D–F). The LCO were cultured in Matrigel domes and showed a spheroid morphology. Immunofluorescence staining for NSCLC specific markers demonstrated robust expression of NAPSIN and CK5 in the established LCO [31] (Fig. 2E, F). In summary, healthy iPSC-derived lung organoids and patient-matched LCO were successfully established in vitro and can be used for comparing the cytotoxic effects of cisplatin alone or loaded onto iPSC-MSC derived EVs.

iPSC-MSC generation and characterization

To produce iPSC-MSC derived EVs, one patient-derived iPSC clone was selected to be differentiated into MSC, and the resulting cell population was characterized. Here, Fib3iPSC cl20 (LC0008) was differentiated into iPSC-MSC following the protocol outlined by [29]. During the differentiation process, iPSC underwent a transition from their characteristic tightly packed colony shape to a loosely packed monolayer within the first week of differentiation (Fig. 3A, d4). Subsequent passages resulted in cells adopting a more spindle-like morphology (Fig. 3A, d14-d35). Fully differentiated iPSC-MSC at day 35 (d35) were expanded and subjected to flow cytometry analysis, while comparing them to their corresponding iPSC clone (Fig. 3B). iPSC-MSC exhibited higher expression of CD90, as measured by mean fluorescent intensity (MFI), compared to their parental iPSC clone. Additionally, iPSC-MSC were positive for the differentiation marker CD105, in contrast to iPSC. Notably, hematopoietic

(See figure on next page.)
Fig. 1 Generation and characterization of iPSC from NSCLC patients. **A** Normal lung fibroblasts were isolated from NSCLC cancer patient operation samples. The purity of isolated fibroblasts were evaluated by staining cells with CD90 and analyzing cells by flow cytometry (grey – unstained control, red – stained with CD90 antibody). CD90+ fibroblasts were cultured for 3–4 passages followed by infection with Sendai virus carrying the OSKM factors. Transduced fibroblasts were cultured on MEFs for 2 weeks. Single colonies were picked onto geltrex coated plates. For each patient, the total number of picked colonies and number of clones with normal karyotype are listed in the table. **B**, **C** Established iPSC were characterized by immunofluorescence staining. iPSC shows expressions of OCT4, TRA1-60, NANOG and SSEA4. Representative images of Fib3iPSC cl20 (B) and Fib2iPSC cl16 **C** are shown. **D**, **E** Patient-derived iPSC show a normal male karyotype. A representative karyogram of Fib3iPSC cl20 (**D**) and Fib2iPSC cl16 (**E**) is shown. **F**, **G** Patient-derived iPSC were differentiated into mesoderm, endoderm and ectoderm. RNA was isolated, qPCR was performed and fold expression ($2^{-\Delta\Delta Ct}$) was calculated. OCT4 was used as a pluripotency marker. Brachyury (T) and Eomes were used as mesodermal markers. FoxA2 and Sox17 were used as endodermal markers. PAX6 and NESTIN were used as ectodermal markers. Additionally, PAX6 was used as negative control in the mesoderm differentiation while Eomes was used as negative control in the ectodermal differentiation. Gene expression for Fib3iPSC cl20 (**F**) and Fib2iPSC cl16 (**G**) is shown. Fold expression was normalized for each row and z-score for the normalized rows was plotted. Black squares represent missing values (n = 1). **H**, **I** Established iPSC clones of LC008 (**H**) and LC0001 (**I**) were analyzed for the presence of Sendai virus genome and the transgenes. Passages at which iPSC clones were tested are indicated. Infected fibroblast on day 7 post infection was used as positive control. Shown are cropped gels images for each PCR. Full-length gels are presented in Supplementary file 1: Fig. 2. Expected band sizes are the following: Sendai virus genome (SeV)—181 bp; vector carrying the transgenes *KLF4*, *OCT4*, *SOX2* (KOS)—528 bp; vector carrying the transgene *KLF4*—410 bp and the vector carrying the transgene *C-MYC*—532 bp (n = 1)
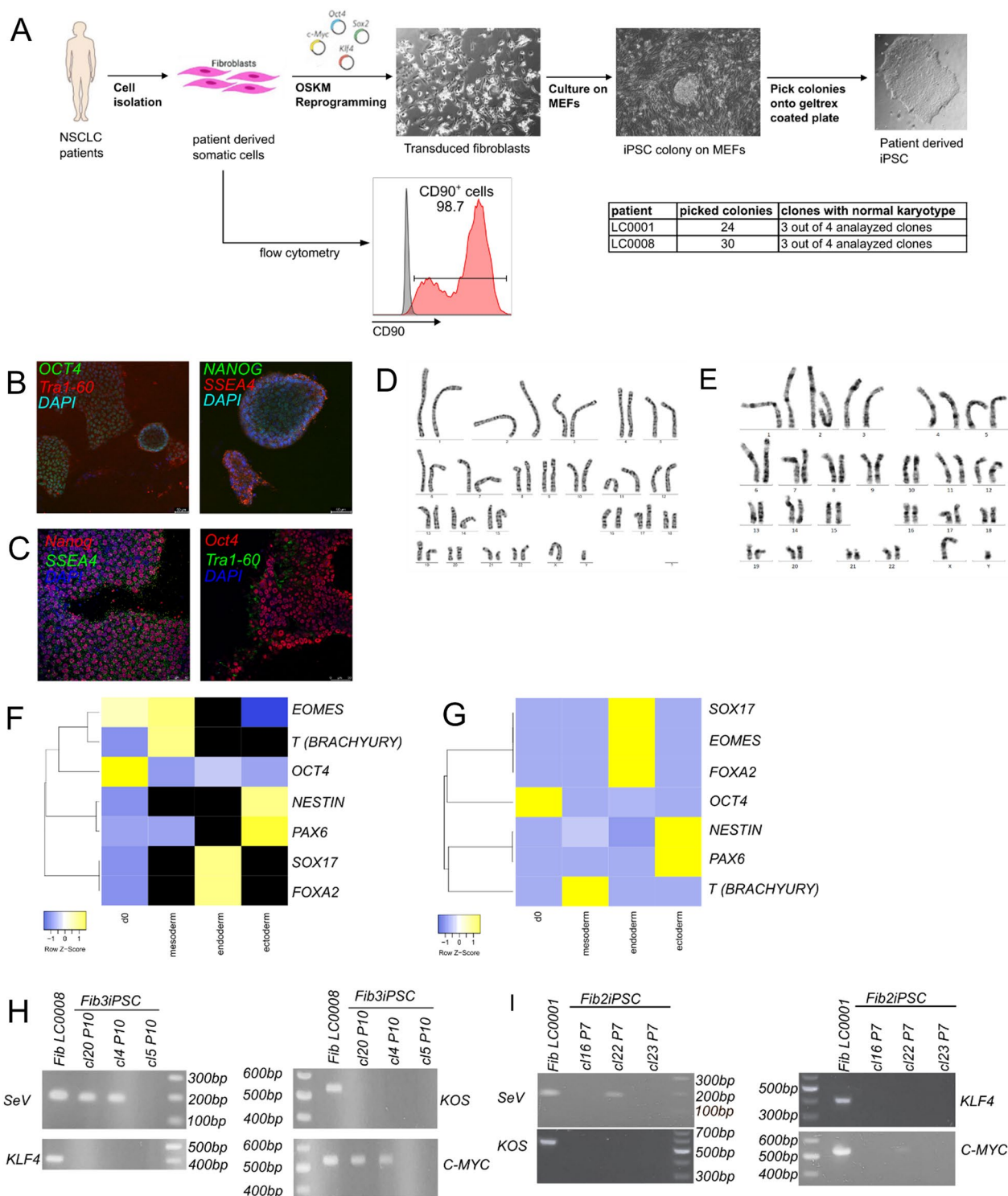
Fig. 1 (See legend on previous page.)

differentiation markers like CD14, CD34 and CD45 were negative in both iPSC-MSC and iPSC, confirming the correct cell identity of the generated patient-derived iPSC-MSC. Furthermore, *OCT4* expression was downregulated in patient-derived iPSC-MSC compared to their corresponding iPSC clone (Fig. 3C). However, *OCT4* expression remained higher in iPSC-MSC than in fully differentiated patient-derived fibroblasts.
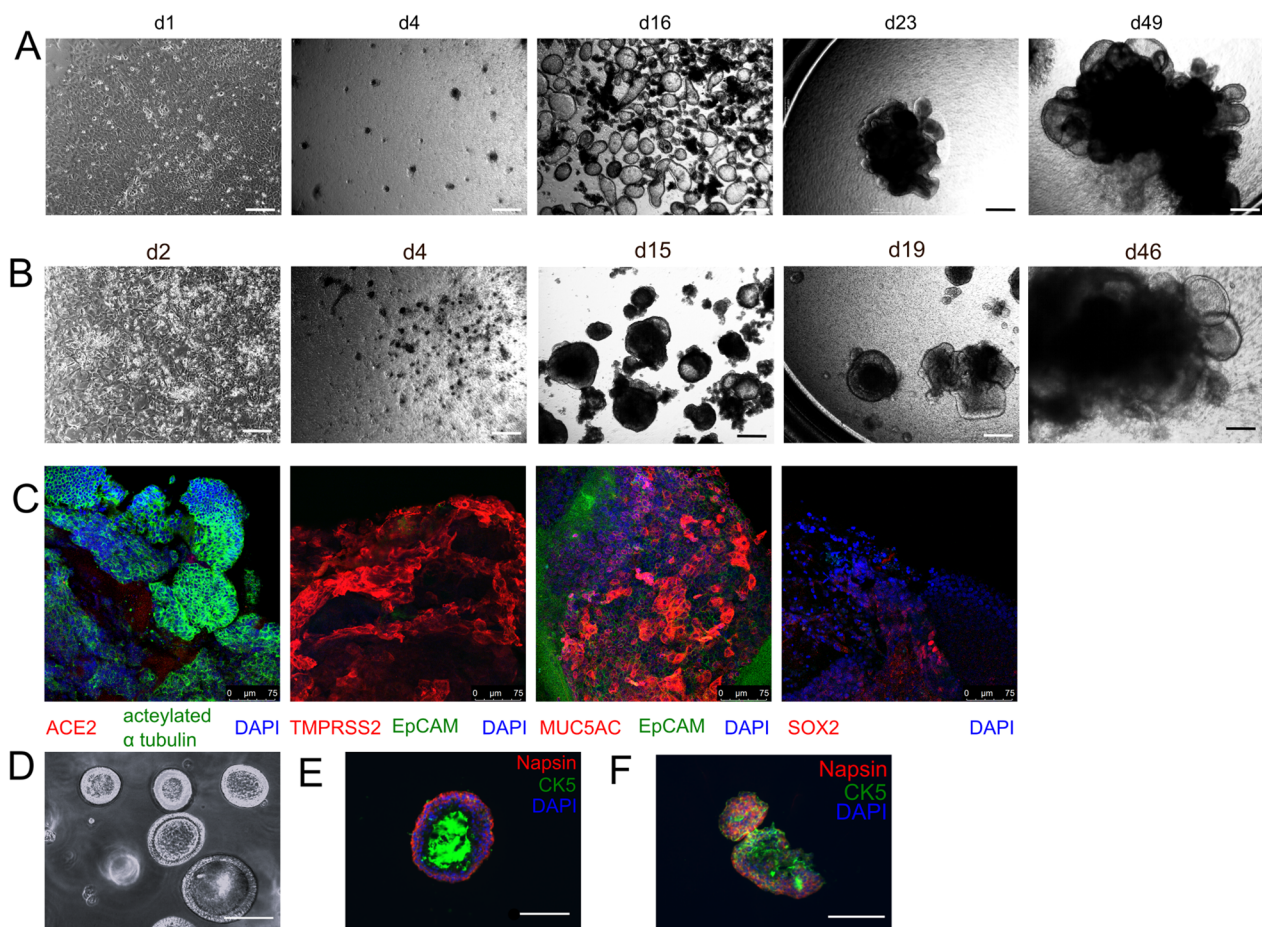
Fig. 2 Branching Lung organoid differentiation from Fib3iPSC cl20. **A**, **B** Fib3iPSC cl20 (**A**) and Fib2iPSC cl16 **B** were induced to differentiate into branching lung organoids (BLO). Representative images of the definitive endoderm (d1 and d2), forming anterior foregut endoderm (AFE) buds (d4), AFE buds in suspension (d15 and d16) and the developing branching lung organoids in a matrigel sandwich (d19—d49). Scale bar represents 1000 μm. **C** LC0008 BLO were picked from matrigel sandwich, washed, minced and stained with antibodies against ACE2, acetylated tubulin, TMPRSS2, EpCAM, MUC5AC and SOX2 for immunofluorescence analysis. Counterstain was performed for Hoechst. Scale bar represents 75 μm. **C** Shown is a representative image of cultured LCO from LC0008 (scale bar = 100 μm). **D** LCO were embedded in paraffin blocks, slices were generated and stained for Napsin and CK5. Shown are representative immunofluorescence images of LC0008 LCO **E** and LC0001 LCO **F**. DAPI was used as a counterstain for DNA (scale bar = 100 μm)

Tri-Lineage differentiation of patient-derived iPSC-MSC successfully differentiated into chondrocytes, with lower degrees of adipogenic and osteogenic differentiation observed (Fig. 3D). As iPSC-MSC were intended for EV production loaded with cisplatin, their cell viability and cytotoxicity were analyzed in response to increasing concentrations of cisplatin (Fig. 3E). Notably, only the two highest cisplatin concentrations of 50 μg/mL and 100 μg/mL resulted in a decline in cell viability and a significant increase in cytotoxicity. Due to the limited in vitro lifespan of iPSC-MSC, cell numbers were recorded over passages. The total accumulated cell number and doubling time was calculated. As shown in Fig. 3F, iPSC-MSC exhibited exponential growth between passage 4 and 9.

However, at passage 10, cell growth started to decelerate, reflected in the increased doubling time from passage 9 to passage 11 (Fig. 3G). In summary, we selected iPSC-MSC passages 4- 9 to be suitable for EV production and isolation.

Characterization of iPSC-MSC derived EV

To generate EVs, iPSC-MSC (P4-P9) from patient LC0008 were expanded in T175 flasks. During each medium change, the medium containing EVs was collected, and after separating cell debris from the medium, EVs were isolated and concentrated. For loading EVs with cisplatin, 20 μg/mL cisplatin was added to the medium for 48 h, followed by EV isolation similar to non-loaded
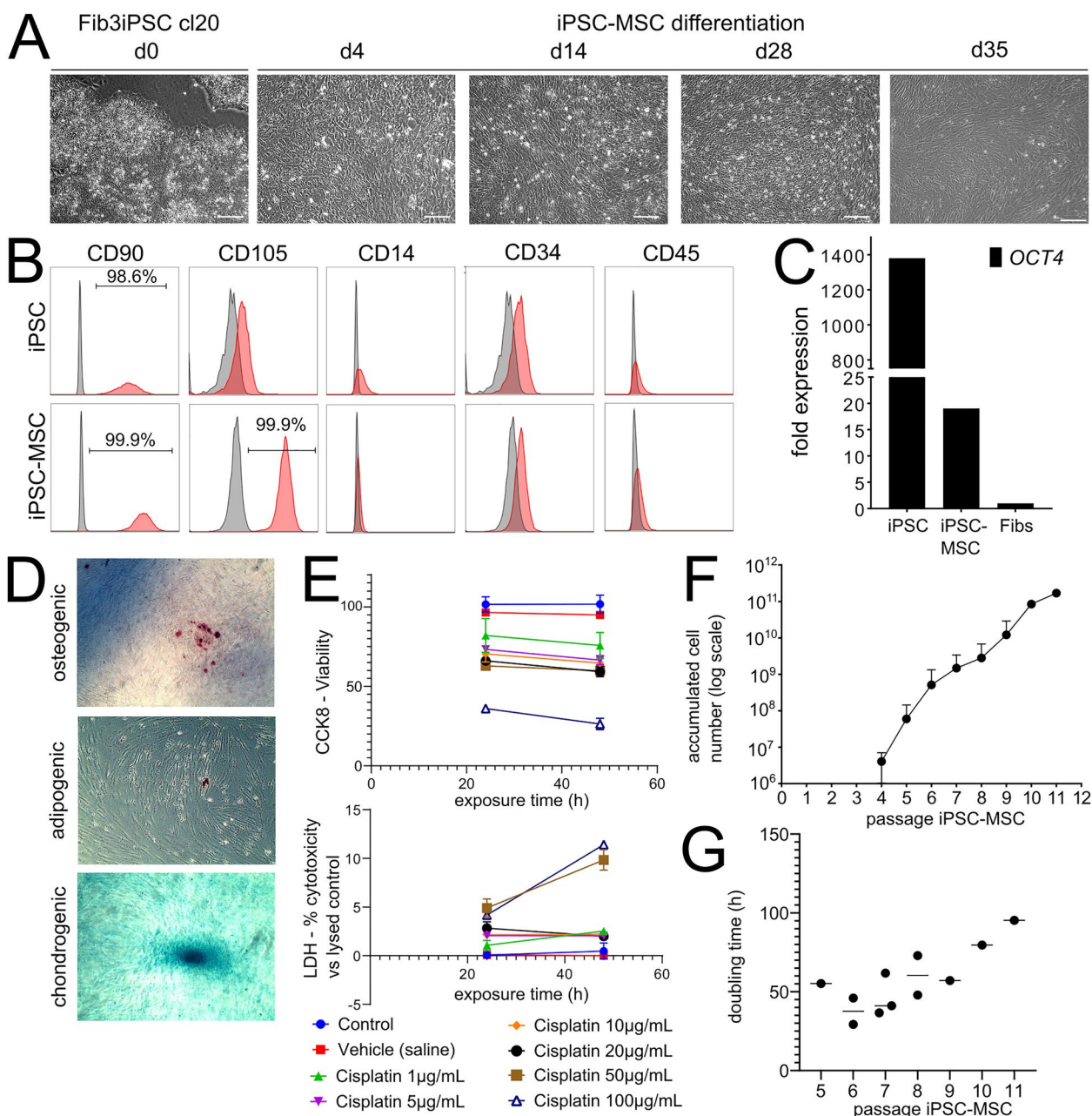
Fig. 3 Generation of iPSC-MSC and iPSC-MSC derived EVs. LC0008 iPSC were induced to differentiate into iPSC-MSC. **A** Shown are representative images of the iPSC before induction (d0) and during the differentiation (d4, d14, d28 and d35). From d35 of differentiation, iPSC-MSC were expanded and used for EV production. Scale bar represents 400 μm. **B** iPSC-MSC and the parental iPSC clone were stained with antibodies against CD90, CD105, CD14, CD34 and CD45 and analyzed with flow cytometry (grey – unstained control, red – stained with specific antibody). **C** *OCT4* expression of iPSC, iPSC-MSC and fibroblasts from LC0008 was checked via qPCR. Fold expression ($2^{-\Delta\Delta Ct}$) compared to the fibroblasts was plotted (n = 1). **D** Osteogenic, adipogenic and chondrogenic differentiation of iPSC-MSC was induced (n = 3). **E** Cytotoxicity of cisplatin in iPSC-MSC was tested in a CCK8 and LDH assay. Viability and % cytotoxicity was plotted (n = 3). **F** Cell numbers of iPSC-MSC during passaging were recorded and the accumulated cell numbers were plotted as logarithmic scale (n = 3). **G** Doubling time during iPSC-MSC culture was calculated and is shown here (n = 1–3)

EVs. EVs were characterized using transmission electron microscopy (TEM) and double-sandwich ELISA (dsELISA). TEM images showed various sizes of isolated EVs (Fig. 4A). Nanoparticle tracking analysis (NTA) analysis showed no significant difference in size of the different isolated EVs. Notably, EVs loaded with cisplatin
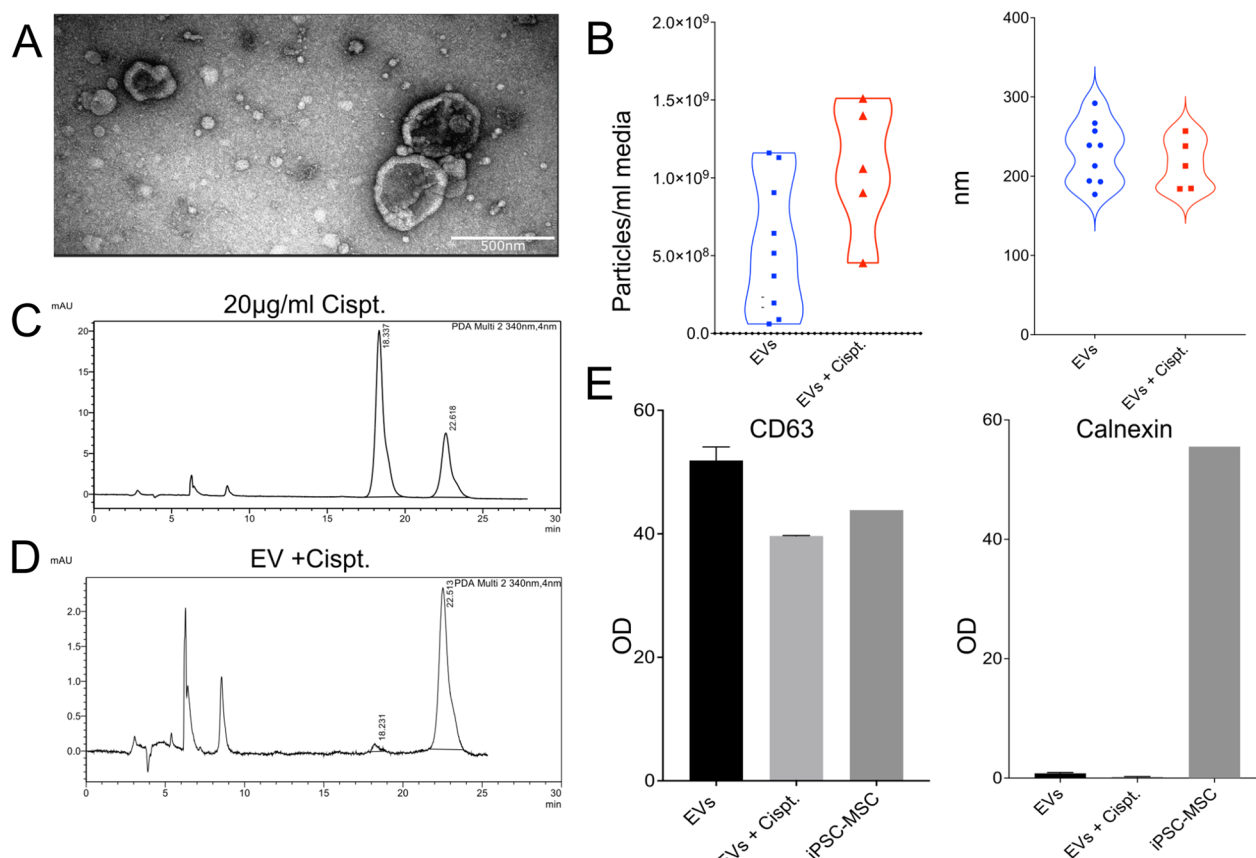
Küstermann *et al. Stem Cell Research & Therapy*   (2024) 15:246

Page 9 of 15

Fig. 4 Characterization of MSC-EVs. **A** TEM image showing EVs with their typical cup-shaped morphology. **B** Violin Plots showing the total amount of EVs per ml of cell media and the size distribution of EVs, both without cisplatin (n = 9) and with encapsulated cisplatin (n = 5). Mann–Whitney test was used to assess differences among groups. There were no significant differences between the groups. **C** HPLC images of 20 µg/mL cisplatin and EVs encapsulated with cisplatin. **D** dsELISA of CD63 (n = 3) and Calnexin (n = 1) in EVs encapsulated with cisplatin and iPSC-MSC. OD: Optical density ratio

(EVs + cispt) contained more particles/mL compared to unloaded EVs (Fig. 4B). However, statistical analysis showed no significant difference.

Further analysis using HPLC (Fig. 4C, D) demonstrated that cisplatin alone displayed peaks at 18 min and 22 min retention time (Fig. 4C). When EVs + cispt were analyzed, a small peak at 18 min retention time was observed (Fig. 4D). Calculating the area under the curve for the 18-min peak indicated that EVs were loaded with 0.07 µg/mL of cisplatin. Subsequently, iPSC-MSC and their derived EVs + cispt and empty EVs were analyzed with a dsELISA (Fig. 4E). CD63, commonly used as a positive marker for EV characterization, was expressed at approximately the same levels in all tested samples, EVs + cispt, MSC-EV and iPSC-MSC. Furthermore, the endoplasmic reticulum protein calnexin used as a negative marker for EVs [32] was absent in isolated EVs + cispt, indicating a pure population of EVs (Fig. 4E). In summary, EVs were successfully isolated from iPSC-MSC and loaded with 0.07 µg/mL cisplatin. These EVs, along with non-loaded EVs,

were used in the subsequent step to treat iPSC-derived BLO and patient-matched LCO.

iPSC-derived organoids and patient-matched lung *cancer* organoids were exposed to EVs

To evaluate the effect of autologous EVs encapsulated cisplatin, BLO and LCO were lysed after 48 h of MSC-EV, EV + cispt and cisplatin exposure, RNA isolated and RT-qPCR performed. To evaluate the cytotoxic effects of these treatments, CCK8 and LDH assays were performed. As shown in Fig. 5A EV induced LDH release in LCO after 48 h exposure. EV treatment alone induced cytotoxic response in BLO, in comparison to LDH positive control (Fig. 5C), however the response was not as pronounced as in LCO. As expected, exposure to 20 µg/mL cisplatin has a tendency to increase metabolic activity of LCO after 24 and 48 h (Fig. 5A) which is also in line with the upregulation of apoptosis related genes (Fig. 5E). Although, to reach statistical significance, it is crucial to increase the sample size. The metabolic

activity of each treatment was checked using CCK8. To this end, the baseline metabolic activity was recorded before the treatments and after 48 h of treatment. Next, the change of metabolic activity was plotted for each treatment in comparison with the baseline. None of the treatments—nor EV, nor cisplatin at both doses significantly influenced metabolic activity of LCO and BLO in CCK8 test (Fig. 5B–D). Nevertheless, cisplatin 0.07 µg/mL increased the metabolic activity of BLO by 50% compared to control in CCK8 test, although this dosage of cisplatin in LCO kept the metabolic activity at the base level. Traditionally, the detection of apoptosis is done on protein level. However, due to limitations on cell amount, apoptosis-related genes were chosen that were shown to be regulated due to cisplatin treatment [33]. Analysis of apoptosis related genes, such as *P53*, *FASL* and *CASPASE-7* showed that EV + cispt upregulated the expression of these genes in patient-matched LCO slightly while no changes in expression of the same genes occurred in iPSC-derived BLO (Fig. 5E, F). Although patient-matched LCO showed a slight upregulation in apoptosis related genes when treated with EV + cispt, cytotoxic activity was not detected via LDH assay (Fig. 5A) suggesting that the gene upregulation is not sufficient to induce apoptosis in this condition or that there are other rescue mechanisms. Allogeneic EV + cispt exposure did not alter the expression of *P53* and *CASPASE-7* genes, although increased the expression *FASL* gene (Fig. 5G). Treatment with autologous EVs has no effect on apoptosis related genes in BLO and no change to even a downregulation in LCO (Fig. 5E, F). Notably, allogenic EV treatment of patient LC0001 BLO remarkably increased *FASL* gene expression (Fig. 5G). Moreover, 20 µg/mL cisplatin upregulated *P53*, *FASL* and *CASPASE-7* in both LCO and *CASPASE-7* in BLO. However, upregulation of *CASPASE-7* was roughly 100× stronger in LCO than in BLO.

Discussion

Testing patient-specific drug responses before initiating chemotherapy for non-small cell lung cancer (NSCLC), is paramount for optimizing therapeutic efficacy and minimizing adverse effects. Traditional two-dimensional (2D) in vitro models have been the cornerstone of chemotherapeutic drug testing; however, they fall short in representing the complex in vivo tumor microenvironment and therefore often yield non-predictive results [34]. The development and use of cancer patient-specific cancer and healthy tissue organoids as a testing platform have been transformative. Studies have shown that patient-derived organoids can faithfully recapitulate patient responses to chemotherapy and are instrumental in guiding personalized treatment decisions [19, 34]. In this study, we have successfully isolated cancer organoids from NSCLC patients tumor biopsy, generated lung organoids, differentiated from patient-specific iPSC. Additionally, autologous cisplatin loaded EVs were obtained from iPSC-MSC and were subsequently administered to both lung and cancer-derived organoids to assess the cytotoxic efficacy of the EV loaded drug in comparison to empty EVs and drug itself. Therefore here we demonstrated methodological benefits, flaws and feasibility for such personalized tests in future.

LCO were isolated from patient-derived tumor biopsies following [27] protocol for generation of lung adenocarcinoma organoids from clinical samples. This study had a success rate of 63% of LCO generation (9 out of 14 patient samples). The success rate of cancer organoid generation from biopsies varies depending on the type of cancer and the method used for organoid creation. For example, a study on pancreatic cancer found that organoids could be successfully created from biopsies in 70–79% of cases [35] and lung cancer organoids at a success rate of 79–80% [36]. However, other studies have reported lower success rates for establishing tumor organoids from biopsies, with some reporting rates as low as 17% [37]. Factors that can affect success rates include the amount and quality of starting material, the presence of normal tissue contamination, and the ability of cells to adapt to in vitro conditions quickly enough to avoid senescence [38]. Overall, while organoids have shown great potential for cancer research and personalized medicine, further research is needed to optimize the process of organoid generation and increase success rates. Lung cancer organoids might be suitable for personalized medicine and as a tool for clinical practice as these can be established fairly quickly and with a small biopsy. A negative effect of the selective treatment on the surrounding cells for the particular patient can be established when using organoids established from adult stem cells. The limiting factor for iPSC-derived lung organoids is the time

(See figure on next page.)
Fig. 5 Cisplatin and Cisplatin loaded EV treatment on iPSC-derived BLO and patient-derived LCO. Patient-derived lung cancer organoids (LCO) and branching lung organoids (BLO) were treated with cisplatin, autologous EV and allogeneic EVs. **A**, **B** Patient-derived LCO were treated with autologous EVs followed by **A** LDH (n = 3) and **B** CCK8 measurement (n = 3). **C**, **D** Patient-derived BLO were treated with autologous EVs followed by **C** LDH (n = 3–4) and **D** CCK8 measurement (n = 5–6). **E**–**G** Fold expression of apoptosis related genes (*P53*, *FASL*, *CASPASE7*) for (**E**) patient-derived LCO (n = 1–2), **F** iPSC-derived BLO (n = 2) treated with allogeneic EVs and **G** iPSC-derived BLO (n = 1) treated with autologous EVs
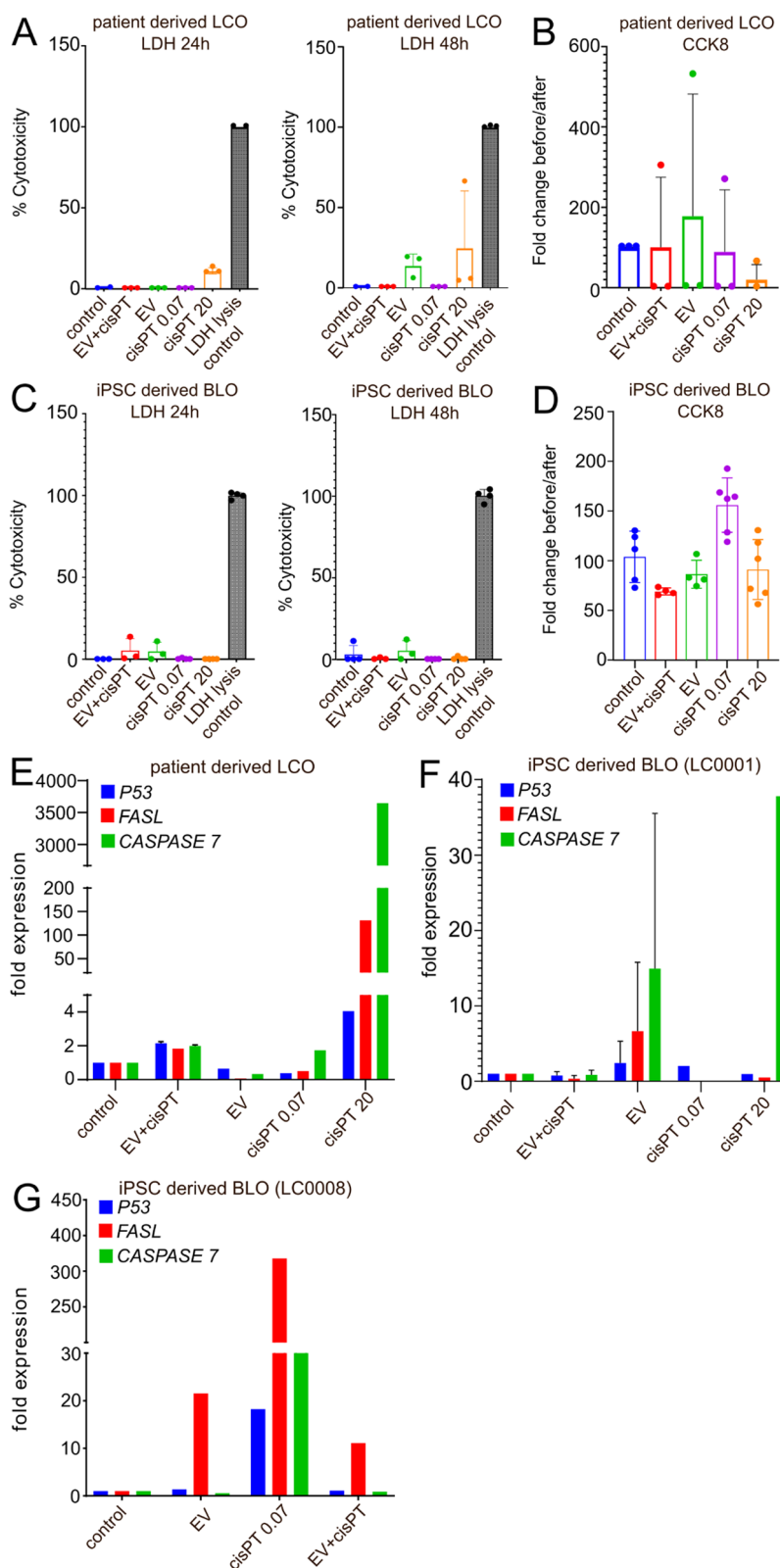
Fig. 5 (See legend on previous page.)

Küstermann *et al. Stem Cell Research & Therapy*   (2024) 15:246

Page 12 of 15

frame of reprogramming and the time frame of branching lung differentiation of 40–60 days. Shorter differentiation protocols have been published however, these focus on a specific cell type, like alveolar type (AT) 2 cells [39]. The alternative applications for iPSC-derived lung organoids are in the field of cytotoxicity tests for novel lung cancer drug candidates as a supplement or substitute to animal models. Furthermore, lung organoids are being used in infectious disease modeling. Recent SARS-CoV2 studies have been using iPSC-derived organoids or patient-derived organoids for elucidating SARS-CoV2 infectivity and drug discovery [40–42]. iPSC-derived organoids could be used to study oncogenesis for a particular cancer type. It is not known what and how normal cells transform into lung cancer cells. Overexpression of candidate genes might give insight into the transformation of normal lung cells into cancer cells. Finally, iPSC organoids are used to study lung fibrosis [43, 44].

The generation of iPSCs from NSCLC patient-derived lung fibroblasts was carried out following protocol by Takahashi et al., 2007 [28]. In contrast to the protocol by Takahashi et al., 2007 this study used commercially available Sendai virus vectors carrying the reprogramming factors instead of lentiviral vectors. Sendai viral vectors cannot integrate into DNA of the host cell leaving no footprint after iPSC are established [45]. Our protocol initiated with the acquisition and dissociation of healthy lung tissue from NSCLC patients, followed by the identification of lung fibroblasts through CD90 expression. The high fidelity of this identification (98% of cells expressing CD90) underscores the precision of our cellular selection for reprogramming [46]. CD90 is defined as a fibroblast marker, however, it is not a selective marker as it is expressed on various cells, including MSC, hematopoietic stem cells, fibroblasts, neurons, and activated endothelial cells [47] but also on iPSC [48]. To more accurately define the fibroblast subtype that is reprogrammed, markers like Vimentin or alpha smooth muscle Actin could be used [47]. As fibroblasts were isolated from cancer patients for this study, cells could also be analyzed for the absence of CD49b, CD87 and CD95 which were found on activated cancer-associated fibroblasts [49] to exclude the possibility of reprogramming cancer fibroblasts.

Sendai viruses have a wide range of host cells [50], therefore a less than pure population is no disadvantage for the efficiency of reprogramming. As shown in this study, subsequent transduction with Sendai virus vectors encoding reprogramming factors facilitated the derivation of iPSC colonies, which, upon rigorous characterization, confirmed their pluripotency and genetic stability. This is a critical validation point, as it ensures that iPSCs retain the necessary features for accurate disease modeling and drug response analysis. Furthermore,

the successful differentiation of iPSCs into trilineage differentiation and the downregulation of the pluripotency marker *OCT4* during differentiation are indicative of the robustness of differentiation protocols used [51, 52]. Although the generation of iPSC is fully established and the time scale of 1–2 months for generation a new iPSC line might be acceptable, however the characterization of each iPSC line is time and cost intensive which makes using iPSC unsuitable for personalized approaches [53]. Furthermore, subsequent differentiations of iPSC range between 1 week for endothelial cells [54], 35 days for iPSC-MSC [28] or 50–80 days for branching lung organoids [55]. Additionally, some mature organoids like lung organoids cannot be cryopreserved, making a constant need for differentiation a necessity for drug testing.

Differentiation of Fib3iPSC cl20 (LC0008) into iPSC-MSC was performed according to the protocol by [28]. Although the differentiation of this clone was successful and efficient, the differentiation time of 35 days for iPSC-MSC and subsequent EV isolation is time consuming. To isolate enough EV and EV + cispt, iPSC-MSC needed to be expanded to 40 × T175 flasks which are hard to manage. Subsequent EV isolation from the cell culture medium and EV concentration takes 24 h and needs to be done in a timely manner without any stops. This poses a problem for using autologous EV from multiple patients. Therefore, this study used autologous EVs from LC0008 and treated patient-derived BLO and LCO from the same patient. Furthermore, an allogeneic EV treatment on patient-derived BLO was assessed. It might be suggested that iPSC-derived MSC EVs exert an increased metabolic activity in LCO. However, due to low cell amount and the few replicates done in this study, there is no definitive conclusion on the effect of autologous EVs on LCO. An increase in replicates might give more clarity into this effect. Additionally, an increase in EVs added to the LCO might be beneficial to show the difference in the metabolic effect between control conditions and EV treated conditions. The increased metabolic activity associated with slight LDH increase may be a sign of cell stress response to MSC-EVs. This phenomenon is called the hormesis effect as an overcompensation for mild environmental stress. It can also be described as a cellular or organism adaptive response aimed at restoring balance in homeostasis when exposed to intermittent mild stressors [56, 57]. Another question is whether the matrigel used for the encapsulation of organoids retains some of the LDH released into the medium, thus interfering with the measurement, especially with low cytotoxic responses. EVs ability to penetrate Matrigel embedded organoids could also be of question. Several studies have investigated the EV to interact with organoids. It has been shown that EVs indeed can alter cancer

organoid proliferation and tumorigenesis, as well as can be analyzed [58, 59]. Moreover, the generation of patient-matched lung organoids was randomized, therefore the selected patient might not have been sensitive to cisplatin. Furthermore, cisplatin concentration usually used in vitro is higher than our encapsulated cisplatin. It might be hypothesized that due to the encapsulation of cisplatin into EVs, the delivery of cisplatin is more targeted, thus lower cisplatin amounts might be needed for cell toxic effects, however, results show that it was not sufficient enough to a robust reduction in metabolic activity in patient-matched LCO. The challenge lies in the increase of encapsulated cisplatin.

Differentiation kits streamline the differentiation process and ensure a high efficiency for the targeted cell type. However, due to the long differentiation time into branching lung organoids, medium components are limited to a time frame of 1 month. Therefore, there is a limitation of organoids that can be cultured per patient, limiting the methods used afterwards to low cell input methods such as RT-qPCR. As this study used a chemotherapy agent, the aim was to determine the level of apoptosis in each condition, thus genes regulating apoptosis in response to cisplatin treatment were chosen [33]. Traditionally, apoptosis is regulated on protein level, however these studies showed an upregulation of *P53* and *CAPSASE7* gene expresion after cisplatin treatment. What needs to be taken into consideration is that washing organoids from the Matrigel domes to isolate RNA can result in even lower cell amounts from which RNA could be isolated and less precise measurement of RNA concentration. This might explain the varying effects seen in this study between patient-derived BLO and LCO. Additionally, cisplatin induced apoptosis is not exclusively regulated by gene expression but also by the cleavage of Caspase-3 as shown by immunoblot analysis [60, 61]. However, the large number of organoids required for protein isolation or EVs for the treatment of organoids was not feasible in this study.

EVs have shown great potential as drug delivery vehicles for cancer treatment. Apart from cisplatin, various chemotherapy agents, such as paclitaxel and doxorubicin, have been encapsulated in EVs to improve targeting [62]. Diverse methodologies can be employed in encapsulating chemotherapeutic agents within EVs, for instance, passive and active loading. In a previous study with doxorubicin, passive and active loading methods were compared. Doxorubicin was encapsulated into bone marrow mesenchymal stem cell-derived EVs. For both methods 250 µg EVs and 125 µg doxorubicin were used. Chemotherapy agent was added to previously isolated EV samples in terms of passive loading, while for active loading electroporation and sonication methods were used.

HPLC analysis revealed 90 µg of doxorubicin was encapsulated within EV samples after electroporation method, while using passive loading they noted no distinction between lysed and non-lysed EV samples. This suggests that the signals related to doxorubicin were probably not a result of the drug's encapsulation into EVs but rather a result of a straightforward conjugation with the EVs [63]**.** Moreover, the main flaws of EV-drug loading using electroporation method is that the method has relatively low efficiency and high variability between studies [64]. To note, our EV + cispt sample did not show an increase in EV size. We chose passive loading of cisplatin into MSC-EVs based on previously published protocols that showed chemotherapy drug paclitaxel significantly increase MSC ability to produce EVs encapsulated with the drug and significantly reduce proliferation and viability of breast (MDA-hyb-1), lung (A549) and ovarian (SK-OV-3) cancer cells when compared to empty MSC-EVs [65, 66].

Conclusions
In this study, we established a pipeline in generating iPSC from NSCLC patient fibroblasts, the differentiation of the newly generated iPSC clones into branching lung organoids and iPSC-MSC. Furthermore, we show a pipeline of generating autologous EVs loaded with cisplatin from iPSC-MSC that were used to treat iPSC-derived organoids and lung cancer organoids. However, EV treatment yielded no effect on organoids, likely due to the low number of EVs used and the low cisplatin amount encapsulated in the EVs. Furthermore, due to the time and labor-intensive processes this pipeline might not be used for personalized approaches.

Supplementary Information

Author contributions
Caroline Kustermann: iPSC generation, Collection and/or assembly of data, Data analysis and interpretation, Manuscript writing. Karīna Narbute: Collection and/or assembly of data, Data analysis and interpretation, Manuscript writing. Valērija Movčana: Collection and/or assembly of data, Manuscript writing. Vadims Parfejevs: Collection and/or assembly of data. Fēlikss Rūmnieks: Immunofluorescence and confocal microscopy, Manuscript writing. Pauls Kauķis: Collection and/or assembly of data. Miks Priedols: Collection and/or assembly of data. Rihards Mikilps-Mikgelbs: Patient recruitment, provision of study material. Marija Mihailova: Preparing cell samples for karyotyping. Santa Andersone: Karyotyping. Aigars Dzalbs: Karyotyping. Cristina Bajo Santos: Manuscript writing/reviewing, Data analysis and interpretation. Alvils Krams: Organizing patient sample collection. Arturs Abols: Study Concept and design, Funding acquisition, Manuscript review.

Küstermann *et al. Stem Cell Research & Therapy*   (2024) 15:246

Page 14 of 15

Declarations

Ethics approval and consent to participate
The title of the approved project was 'Testing of patient-derived stem cell extracellular vesicles loaded with drugs in a personalised lung cancer-on-a-chip platform'. This study was approved by the Central Medical Ethics committee of Latvia (Medical Ethics No. E 1.1–2/8–6.22–2/37; date of approval: 17.05.2022). All patients gave written informed consent.

Consent for publication
Not applicable.

Conflict of interest
Authors declare no conflict of interest.

Author details
[1]Latvian Biomedical Research and Study Center, Rātsupītes lela 1, Riga 1067, Latvia. [2]Faculty of Medicine, University of Latvia, Jelgavas lela 3, Riga, Latvia. [3]Riga East Clinical University Hospital Center of Tuberculosis and Lung Diseases, Upeslejas, Ropažu Novads, Latvia. [4]IVF Riga Stem Cell Center, Zaļā lela 1, Rīga, Latvia.

References

1. Mattiuzzi C, Lippi G. Current cancer epidemiology. J Epidemiol Glob Health. 2019;9:217–22.
2. Sung H, Ferlay J, Siegel RL, et al. Global cancer statistics 2020: GLOBOCAN estimates of incidence and mortality worldwide for 36 cancers in 185 countries. CA Cancer J Clin. 2021;71:209–49.
3. Padinharayil H, Varghese J, John MC, et al. Non-small cell lung carcinoma (NSCLC): implications on molecular pathology and advances in early diagnostics and therapeutics. Genes Dis. 2023;10:960–89.
4. Dama E, Colangelo T, Fina E, et al. Biomarkers and lung cancer early detection: state of the art. Cancers. 2021;13:3919.
5. Yuan M, Huang L-L, Chen J-H, et al. The emerging treatment landscape of targeted therapy in non-small-cell lung cancer. Signal Transduct Target Ther. 2019;4:1–14.
6. Kryczka J, Kryczka J, Czarnecka-Chrebelska KH, et al. Molecular mechanisms of chemoresistance induced by cisplatin in NSCLC cancer therapy. Int J Mol Sci. 2021;22:8885.
7. Nagano T, Tachihara M, Nishimura Y. Molecular mechanisms and targeted therapies including immunotherapy for non-small cell lung cancer. Curr Cancer Drug Targets. 2019;19:595–630.
8. Buzás EI, Tóth EÁ, Sódar BW, et al. Molecular interactions at the surface of extracellular vesicles. Semin Immunopathol. 2018;40:453–64.
9. Yáñez-Mó M, Siljander PR-M, Andreu Z, et al. Biological properties of extracellular vesicles and their physiological functions. J Extracell Vesicles 2015;4:27066.
10. Herrmann IK, Wood MJA, Fuhrmann G. Extracellular vesicles as a next-generation drug delivery platform. Nat Nanotechnol. 2021;16:748–59.
11. Goh WJ, Lee CK, Zou S, et al. Doxorubicin-loaded cell-derived nanovesicles: an alternative targeted approach for anti-tumor therapy. Int J Nanomed. 2017;12:2759–67.
12. Maumus M, Rozier P, Boulestreau J, et al. Mesenchymal stem cell-derived extracellular vesicles: opportunities and challenges for clinical translation. Front Bioeng Biotechnol 2020;8.
13. Linero I, Chaparro O. Paracrine effect of mesenchymal stem cells derived from human adipose tissue in bone regeneration. PLoS ONE. 2014;9: e107001.
14. Gowen A, Shahjin F, Chand S, et al. Mesenchymal stem cell-derived extracellular vesicles: challenges in clinical applications. Front Cell Dev Biol 2020;8.
15. Lo Sicco C, Reverberi D, Balbi C, et al. Mesenchymal stem cell-derived extracellular vesicles as mediators of anti-inflammatory effects: endorsement of macrophage polarization. Stem Cells Transl Med. 2017;6:1018–28.
16. Srivastava A, Rathore S, Munshi A, et al. Organically derived exosomes as carriers of anticancer drugs and imaging agents for cancer treatment. Semin Cancer Biol. 2022;86:80–100.
17. Zhang W, Ling Y, Sun Y, et al. Extracellular vesicles derived from mesenchymal stem cells promote wound healing and skin regeneration by modulating multiple cellular changes: a brief review. Genes. 2023;14:1516.
18. Kapałczyńska M, Kolenda T, Przybyła W, et al. 2D and 3D cell cultures – a comparison of different types of cancer cell cultures. Arch Med Sci AMS. 2018;14:910–9.
19. Sachs N, de Ligt J, Kopper O, et al. A living biobank of breast cancer organoids captures disease heterogeneity. Cell. 2018;172:373-386.e10.
20. Kim M, Mun H, Sung CO, et al. Patient-derived lung cancer organoids as in vitro cancer models for therapeutic screening. Nat Commun. 2019;10:3991.
21. Kondo J, Inoue M. Application of cancer organoid model for drug screening and personalized therapy. Cells. 2019;8:470.
22. Drost J, Clevers H. Organoids in cancer research. Nat Rev Cancer. 2018;18:407–18.
23. Gorain B, Bhattamishra SK, Choudhury H, et al. Overexpressed receptors and proteins in lung cancer. Nanotechnol.-Based Target. Drug Deliv. Syst. Lung Cancer: Elsevier; 2019. p. 39–75.
24. Komuro H, Aminova S, Lauro K, et al. Design and evaluation of engineered extracellular vesicle (EV)-based targeting for EGFR-overexpressing tumor cells using monobody display. Bioengineering. 2022;9:56.
25. Li Y-J, Wu J-Y, Hu X-B, et al. Autologous cancer cell-derived extracellular vesicles as drug-delivery systems: a systematic review of preclinical and clinical findings and translational implications. Nanomed. 2019;14:493–509.
26. Shi D, Mi G, Wang M, et al. In vitro and ex vivo systems at the forefront of infection modeling and drug discovery. Biomaterials. 2019;198:228–49.
27. Li Z, Yu L, Chen D, et al. Protocol for generation of lung adenocarcinoma organoids from clinical samples. STAR Protoc. 2020;2: 100239.
28. Takahashi K, Tanabe K, Ohnuki M, et al. Induction of pluripotent stem cells from adult human fibroblasts by defined factors. Cell. 2007;131:861–72.
29. Frobel J, Hemeda H, Lenz M, et al. Epigenetic rejuvenation of mesenchymal stromal cells derived from induced pluripotent stem cells. Stem Cell Rep. 2014;3:414–22.
30. Toro-Córdova A, Ledezma-Gallegos F, Mondragon-Fuentes L, et al. Determination of liposomal cisplatin by high-performance liquid chromatography and its application in pharmacokinetic studies. J Chromatogr Sci. 2016;54:1016–21.
31. Zhao W, Wang H, Peng Y, et al. ΔNp63, CK5/6, TTF-1 and napsin A, a reliable panel to subtype non-small cell lung cancer in biopsy specimens. Int J Clin Exp Pathol. 2014;7:4247–53.
32. Lobb RJ, Becker M, Wen SW, et al. Optimized exosome isolation protocol for cell culture supernatant and human plasma. J Extracell Vesicles 2015;4.
33. Yang C, Kaushal V, Haun RS, et al. Transcriptional activation of caspase-6 and -7 genes by cisplatin-induced p53 and its functional significance in cisplatin nephrotoxicity. Cell Death Differ. 2008;15:530–44.
34. Vlachogiannis G, Hedayat S, Vatsiou A, et al. Patient-derived organoids model treatment response of metastatic gastrointestinal cancers. Science. 2018;359:920–6.
35. Tiriac H, Carlos Bucobo J, Tzimas D, et al. Successful creation of pancreatic cancer organoids by means of EUS-guided fine-needle biopsy for personalized cancer treatment. Gastrointest Endosc. 2018;87:1474–80.
36. Hu Y, Sui X, Song F, et al. Lung cancer organoids analyzed on microwell arrays predict drug responses of patients within a week. Nat Commun. 2021;12:2581.
37. Xu H, Jiao D, Liu A, et al. Tumor organoids: applications in cancer modeling and potentials in precision medicine. J Hematol OncolJ Hematol Oncol. 2022;15:58.

38. Foo MA, You M, Chan SL, et al. Clinical translation of patient-derived tumour organoids- bottlenecks and strategies. Biomark Res. 2022;10:10.
39. Bluhmki T, Traub S, Müller A-K, et al. Functional human iPSC-derived alveolar-like cells cultured in a miniaturized 96-Transwell air–liquid interface model. Sci Rep. 2021;11:17028.
40. Bose B. Induced pluripotent stem cells (iPSCs) derived 3D human lung organoids from different ethnicities to understand the SARS-CoV2 severity/infectivity percentage. Stem Cell Rev Rep. 2021;17:293–5.
41. Giani AM, Chen S. Human pluripotent stem cell-based organoids and cell platforms for modelling SARS-CoV-2 infection and drug discovery. Stem Cell Res. 2021;53: 102207.
42. Spitalieri P, Centofanti F, Murdocca M, et al. Two different therapeutic approaches for SARS-CoV-2 in hiPSCs-derived lung organoids. Cells. 2022;11:1235.
43. Chen Y-W, Huang SX, de Carvalho ALRT, et al. A three-dimensional model of human lung development and disease from pluripotent stem cells. Nat Cell Biol. 2017;19:542–9.
44. Strikoudis A, Cieślak A, Loffredo L, et al. Modeling of fibrotic lung disease using 3D organoids derived from human pluripotent stem cells. Cell Rep. 2019;27:3709-3723.e5.
45. Chen I-P, Fukuda K, Fusaki N, et al. Induced pluripotent stem cell reprogramming by integration-free sendai virus vectors from peripheral blood of patients with craniometaphyseal dysplasia. Cell Reprogramming. 2013;15:503–13.
46. Mack AA, Kroboth S, Rajesh D, et al. Generation of induced pluripotent stem cells from CD34+ cells across blood drawn from multiple donors with non-integrating episomal vectors. PLoS ONE. 2011;6: e27956.
47. Kisselbach L, Merges M, Bossie A, et al. CD90 Expression on human primary cells and elimination of contaminating fibroblasts from cell cultures. Cytotechnology. 2009;59:31–44.
48. Characterization of Surface Markers and DNA Regulatory Gene Expression during Neutrophil Differentiation from Human Induced Pluripotent Stem Cells. Mol Ther 2011;19:S219.
49. Agorku DJ, Langhammer A, Heider U, et al. CD49b, CD87, and CD95 Are markers for activated cancer-associated fibroblasts whereas CD39 marks quiescent normal fibroblasts in murine tumor models. Front Oncol 2019;9.
50. Nakanishi M, Otsu M. Development of sendai virus vectors and their potential applications in gene therapy and regenerative medicine. Curr Gene Ther. 2012;12:410–6.
51. Kuang Y-L, Munoz A, Nalula G, et al. Evaluation of commonly used ectoderm markers in iPSC trilineage differentiation. Stem Cell Res. 2019;37: 101434.
52. Ward E, Twaroski K, Tolar J. Feeder-free derivation of naive human pluripotent stem cells. Stem Cells Dev. 2017;26:1087–9.
53. Park S, Gwon Y, Khan SA, et al. Engineering considerations of iPSC-based personalized medicine. Biomater Res. 2023;27:67.
54. Hamad S, Derichsweiler D, Gaspar JA, et al. High-efficient serum-free differentiation of endothelial cells from human iPS cells. Stem Cell Res Ther. 2022;13:251.
55. Miller AJ, Dye BR, Ferrer-Torres D, et al. Generation of lung organoids from human pluripotent stem cells in vitro. Nat Protoc. 2019;14:518–40.
56. Bhakta-Guha D, Efferth T. Hormesis: decoding two sides of the same coin. Pharmaceuticals. 2015;8:865–83.
57. Spear LP, Varlinskaya EI. Low dose effects in psychopharmacology: ontogenetic considerations. Nonlinearity Biol Toxicol Med. 2005;3:97–111.
58. Zhang Y, Lu A, Zhuang Z, et al. Can organoid model reveal a key role of extracellular vesicles in tumors? A comprehensive review of the literature. Int J Nanomed. 2023;18:5511–27.
59. Ural EE, Toomajian V, Hoque Apu E, et al. Visualizing extracellular vesicles and their function in 3D tumor microenvironment models. Int J Mol Sci. 2021;22:4784.
60. Henkels KM, Turchi JJ. Cisplatin-induced Apoptosis Proceeds by Caspase-3-dependent and -independent Pathways in Cisplatin-resistant and -sensitive human ovarian cancer cell lines1. Cancer Res. 1999;59:3077–83.
61. Ono K, Sato K, Nakamura T, et al. Reproduction of the antitumor effect of cisplatin and cetuximab using a three-dimensional spheroid model in oral cancer. Int J Med Sci. 2022;19:1320–33.
62. Walker S, Busatto S, Pham A, et al. Extracellular vesicle-based drug delivery systems for cancer treatment. Theranostics. 2019;9:8001–17.
63. Mukhopadhya A, Tsiapalis D, McNamee N, et al. Doxorubicin loading into milk and mesenchymal stem cells' extracellular vesicles as drug delivery vehicles. Pharmaceutics. 2023;15:718.
64. Sutaria DS, Badawi M, Phelps MA, et al. Achieving the promise of therapeutic extracellular vesicles: the devil is in details of therapeutic loading. Pharm Res. 2017;34:1053–66.
65. Melzer C, Rehn V, Yang Y, et al. Taxol-loaded MSC-derived exosomes provide a therapeutic vehicle to target metastatic breast cancer and other carcinoma cells. Cancers. 2019;11:798.
66. Tran TH, Wang X, Browne C, et al. Wnt3a-induced mesoderm formation and cardiomyogenesis in human embryonic stem cells. Stem Cells Dayt Ohio. 2009;27:1869–78.

Publisher's Note